Mapping Cheshire Cats' Leg: A histological approach of cortical bone tissue through modern GIS technology

Myrto Mallouchou, Loukas Katikas, Elizabeth Stathopoulou, Nikolaos Papaioannou, Nikoleta Varagka & Byron Nakos

Anatomical Science International

ISSN 1447-6959

Anat Sci Int
DOI 10.1007/s12565-019-00503-4

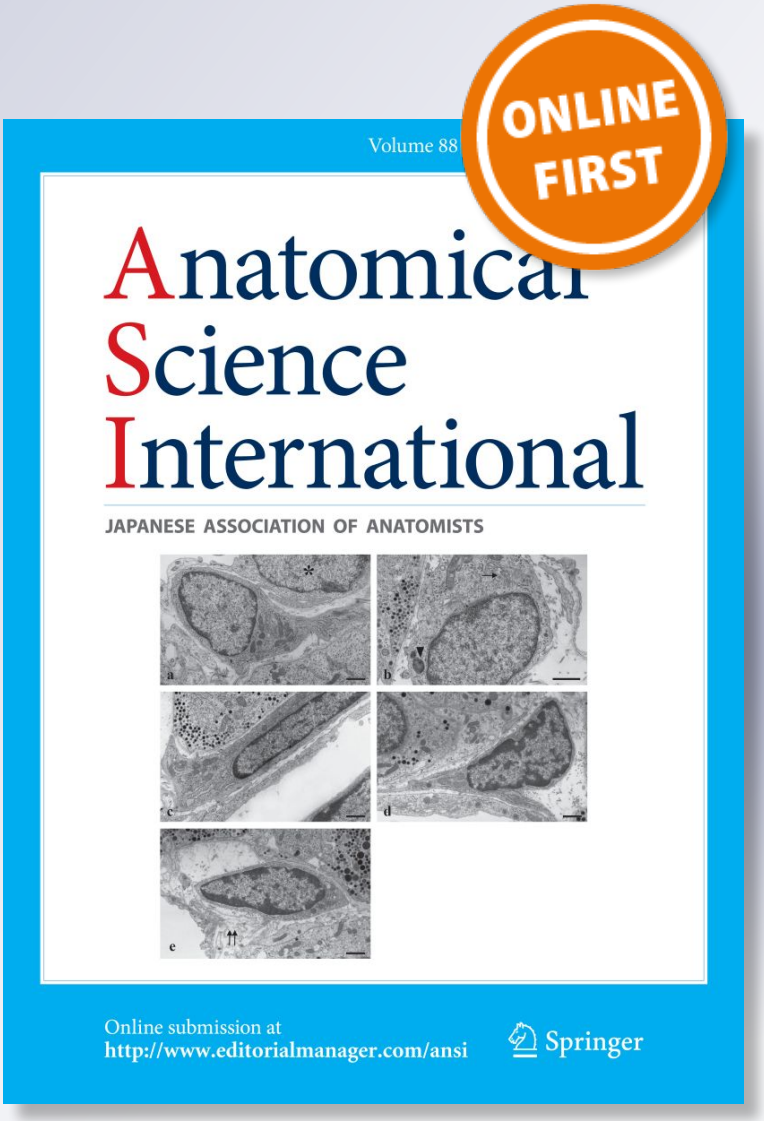

Springer

Anatomical Science International
https://doi.org/10.1007/s12565-019-00503-4

ORIGINAL ARTICLE

Mapping Cheshire Cats' Leg: A histological approach of cortical bone tissue through modern GIS technology

Myrto Mallouchou[1] · Loukas Katikas[2] · Elizabeth Stathopoulou[1] · Nikolaos Papaioannou[3] · Nikoleta Varagka[3] · Byron Nakos[2]

Received: 9 April 2019 / Accepted: 3 September 2019

Abstract

The present study concerns the histological examination of the hind limb of a cat (*Felis* sp.), with an emphasis on Haversian bone. Acknowledging the variety of obstacles to be confronted, during histological studies, it was decided the documentation, description, and comparison of the longitudinal distribution of the main microstructural characteristics. To reveal what remains hidden from the sight of knowledge, the novel Geographical Information Systems (GIS) methodology was followed. In means to provide conclusive and credible results, it was analyzed the full spectrum of the resulted cross sections and not just a statistical acceptable number or a specific region of interest. In addition, having used the right femur and tibia from the same animal, species and age discrepancies were eliminated. More thoroughly, osteon and Haversian canal size and circularity were calculated and spatially analyzed. Absolute and relative osteon population densities (OPDs) and tissue-type distributions were also estimated. The use of GIS software constituted the core of the current research, since its application transformed cross sections into informative maps, where inter-skeletal, inter-cortical, and intra-cortical distributional patterns were directly recognized and accordingly correlated to strain and load regimes. As result, it is provided the histomorphological and histomorphometrical profile of the samples, under the prism of the existing biomechanical regime. Finally, having further deployed the potentials of GIS software, it is verified and promoted the feasibility of histological mapping as an indispensable procedure, aligned with the necessities of modern science, regardless of discipline or background.

Keywords Mammalian bone histology · Histological mapping · Bone histomorphology · Bone histomorphometry · Geographical information systems (GIS)

Introduction

Bone growth and structure

Bone constitutes a complex hierarchically structured entity, where ordered and disordered materials are organized in different forms, so as to produce distinct hierarchical levels. These levels are responsible for the mechanical properties of bone and also for its metabolic and sensing adaptation (Reznikov et al. 2014). The resulted tissue types of bones are not solely the products of the organization of ordered and disordered material, but also of the existing vascularization and cells function. For almost 330 years, scientists are focused in describing, classifying, and comparing these tissue types between them and among vertebrate taxa (Amprino 1947; Enlow and Brown 1956, 1958; Foote 1916; Havers 1691; Jaffe 1929; McFarlin

✉ Myrto Mallouchou
mmalloyc@geol.uoa.gr

[1] Department of Historical Geology and Palaeontology, Faculty of Geology and Geoenvironment, School of Science, National and Kapodistrian University of Athens, University Campus-Zographou, 15784 Athens, Greece

[2] School of Rural and Surveying Engineering, National Technical University of Athens, 9, Heroon Polytechniou Str. Zographos, 15780 Athens, Greece

[3] School of Veterinary Medicine, Faculty of Health Sciences, Aristotle University of Thessaloniki, University Campus, 54124 Thessaloniki, Greece

Published online: 18 September 2019

et al. 2016; Quekett, 1855). It is evident that bones, even those originated from the same organism, usually exhibit a combination of tissue types and during ontogenesis can be altered or replaced by other (secondary) types (Enlow 1963; Enlow and Brown 1956, 1958; Singh et al. 1974). Additional factors that often justify tissue-type diversity within a single skeleton are phylogeny, environment, and load (Currey 2002; Maggiano 2012; Martin et al. 1998).

Long bones are formed during the endochondral ossification of a previously laid cartilaginous tissue. This process is known as modeling, which is predominantly restricted to the growing (and developed) skeleton and accounts for changes in bone size, shape, and the resulted alterations in its length, width, and diameter. Modeling is determined genetically, hormonally, and environmentally. The consequent mechanism is the lifelong process of bone remodeling, which secures the maintenance of the constitutional integrity of bone tissue and homeostasis within the matrix. Simultaneously, it favors the adaptation of bone to biomechanical strains, phylogenetic signals, age maturity (ontogeny), and repair. Remodeling can be either stochastic or targeted, depending on whether its induction is metabolically driven or damage initiated.

Mammals usually exhibit woven, lamellar, fibrolamellar, and Haversian bone. Woven bone is a primary tissue type of mineralization during endochondral ossification, which represents periods of slow growth. Lamellar bone is a better organized structure that can be either of primary origin, representing rapid growth rates, or of secondary origin, replacing existing bone (Amprino and Godina 1947). Haversian systems (also known as secondary osteons and as basic structural units—BSU) constitute the core histomorphological expression of bone remodeling (Martin et al. 1998). The activated osteoclasts and osteoblasts of remodeling are collectively known as Bone Remodeling Units (BRU) or as Basic Multicellular Units (BMU). Haversian systems are created when osteoblasts circularly secrete osteoid, producing lamellae with trapped osteocytes in lacunae. To do so, osteoclasts' activity must have preceded and initiated the formation of the resorptive bay and the consequent "cutting cone" tunnel into the bone matrix (Mescher 2013). This tunnel constitutes the Haversian canal with the rough edged wall, where the osteoblasts begin to operate and, eventually, transform it into a "closing cone". The progressive canal-filling produce, in transverse cross sections, osteons with Haversian canals of different dimensions (diameter). Usually, these structures are distinguished into: developing resorption cavities, forming (or closing) osteons and completed osteons. The described succession of resorption by formation is known as "coupling phenomenon", and it is rather a complex process, unlike the oversimplified model that is usually implied. Although coupling analysis is not between the aims of this paper, Sims' and Martins' review article (2014), is suggested for a thorough understanding of the underlying signals and activities that take place.

It must be emphasized that despite bones' multifunctional role, its dominant feature is its capability to support loads either originating from locomotion or weight-bearing needs. Consequently, this trait is the one that defines the material properties of bone and also its size, shape, and structure both macroscopically and microscopically (Skerry 2006). It was in 1892, when Wolff connected the internal architecture of bones with their function and form (Wolff, 1892). After almost a century, Harold Frost studied the relationship of biomechanics and bone remodeling and proposed the concept of *The Mechanostat* (Frost 1987a) and later *The Utah Paradigm* (Frost 1998a). Although these theories have received great criticism, they are still considered the pillars upon which the deciphering of bone biomechanics is based.

Relevant and contemporary histological perspective

It is scientifically acceptable, as aforementioned, that the structural characteristics of bone (e.g., cross-sectional shape and cortical thickness) are adjusted through the modeling process (Schaffler et al. 1985). On the other hand, remodeling modifies differently the cortical regions of the same cross section to achieve optimum bone organization. Thus, differences in histomorphology that are expressed as porosity, osteon density, shape, and size vary between regions, where distinct biomechanical loading is applied (Kumar et al. 2010). Both these processes ameliorate the mechanical properties of bones by attributing equally to its overall stiffness, strength, fatigue resistance, and toughness. Therefore, osteon population densities and Haversian systems' morphological characteristics are widely selected, in histological studies, as the most significant sub-structures that could enhance the general understanding of bone functional adaptation (Abbott et al. 1996; Mason et al. 1995; Pfeiffer et al. 2006; Robling and Stout 2003; Urbanova and Novotny 2005). More thoroughly, increasing osteon area was correlated with age and body mass (Britz et al. 2009; Felder et al. 2017), whereas it has also been connected with a homeostatic driven calcium supply (Jowsey 1966; Ruth 1953). Osteon size is a trait widely used for species differentiation (Hillier and Bell 2007; Martiniakova et al. 2006). Secondary osteon population density and fractional area, secondary osteon cross-sectional area, shape and orientation, and porosity are only some of the basic histomorphological characteristics that have been used in the context of interpreting load history (Cattaneo et al. 2009; Hillier and Bell 2007; Keenan et al. 2017).

The studies that have examined recent remains of *Felis* sp. compact bone are not many (Hillier and Bell 2007). Whether the description concerns domesticated or wild cats, lamellar,

and Haversian bone were the only observed tissue types. The distribution of these tissues was differed significantly amongst them and between sampling regions, though they shared common histomorphology (Enlow and Brown 1958; Foote 1916; Harsanyi 1993).

Jowsey (1966) studied the Haversian systems in human and some animals, among which six cats, whose osteon mean diameter was 163 ± 30 μm and Haversian canal perimeter was 102 ± 36 μm. Diaz and Rajtova (1975), by measuring two tibiae, showed that the ranges of osteon diameter, in a cat and a wild cat, were 110–155 μm and 90–175 μm, respectively.

The present study is concentrated on providing osteon and Haversian canal area and perimeter measurements and consequently diameter and circularity calculations, whereas Osteon Population Densities (OPDs) are also estimated. Moreover, for the first time, is calculated the percent of each osteon area occupied by its analogous Haversian canal. The last trait discriminates between forming and completed osteons and it can potentially indicate the regions where remodeling process is active. The aforementioned characteristics were chosen since they represent the most commonly used traits in histological studies.

Particularly, the focus of recent research has been directed toward the estimation of osteon circularity and OPD. Circularity (*CI*) is expressed as: $CI = 4\pi(\text{area}/\text{perimeter}^2)$ and constitutes a unitless measurement which has been applied for load-history interpretation, inter-species comparison, and age-at-death estimation (Crescimanno and Stout 2012; Dominguez and Crowder 2012; Goliath et al. 2016). Not all studies were conclusive; nevertheless, circularity is still considered as an important histomorphometrical trait, which is usually included in intra-cortical remodeling research (Keenan et al. 2017). The study of Maggiano et al. (2017) constitutes a step of advancement, since it presents the factors that affect the longitudinal variation of osteon circularity. Nonetheless, the reasons that initiate and/or sustain these differences are equally important and need to be unfold.

OPD is calculated as the number of osteons per square millimeter (Frost 1987b). So far, results have not only shown a strong relationship between chronological age and OPD, but have also considered OPD as an (expressed) adaptation of bone to forces of biomechanical origin (Gocha and Agnew 2016; Kerley 1965; Robling and Stout 2008). Progressively, our study examines if there is an interconnection between osteon circularity and OPD distribution. The importance of this examination was underlined by of Keenan et al. (2017). Previously, it had been suggested by Dominguez and Crowder (2012) and Britz et al. (2009), who observed that circularity can possibly be influenced by OPD local variations. In the current publication, only the intact osteons are counted to provide OPD values.

Despite the above-mentioned traits that are used in bone biomechanical analyses, Skedros et al. (2002, 2006, 2011) vigorously support the opinion that, in the absence of strain data, the most reliable structural characteristics for interpreting load regime in limb bones are Collagen Fiber Orientation (CFO) and osteon morphotypes. He also raises a number of issues to be cautious when studying load history, among which the modeling–remodeling distinction, the load-complexity categories' classification (Keenan et al. 2017), and the skeletal differential growth rates discrimination. Undoubtedly, the impediments that scientist usually confront, during histological studies, are many and the most common of them amplify the charge of the previously cited issues. For example, the limited sampling and/or the extrapolation from only a small number of osteons are some of the obstacles to deal with. In addition, knowing that histological studies apply destructive techniques, at least during the stage of sample preparation, an urge arises to produce results that are both credible and repeatable. Towards this direction, studies are concentrated in obtaining comparable samples from the midshafts of long bones (mainly femurs, tibias, and humerus), when whole bone sections were available and in compliance with the necessary permissions and ethics. Nonetheless, the most encountered approach in literature is the use of either small-sized samples or fragments. Inevitably, the question that emerges is if this limited sampling constitutes a good representative, adequate to attribute its observed and measured characteristics to the whole. Another query that rises concerns the longitudinal distribution of histomorphological traits of bones in a certain organism and at a given instant. This thought resulted from the nature of biomechanical loading, which is neither interrupted nor age and region restricted.

In 2012, Cambra-Moo et al. (2012) and Rose et al. (2012) proposed a novel methodology that would diminished the above-mentioned problems. The use of Geographical Information Systems (GIS) software empowered the histological examination, by allowing the transformation of complete bone sections (retrieved by a microscope) into maps, where the inserted data could be spatially analyzed. Whether demonstrating that through GIS osteon morphotypes could decipher biomechanical loading or establishing compartmentalization mapping to describe ontogenetically induced adaptation, these studies laid the foundations of histological mapping.

The feasible use of GIS methodology sparked our interest to meticulously examine longitudinally the femur and the tibia of the same cat (*Felis* sp.), by documenting, describing, and comparing the most commonly used histological variables and thus further deploying the potentials of this software. Also, having comprehend the aforementioned posed obstacles, during histological studies, as potential resolution

was decided to be followed a holistic histological approach, by analyzing the full spectrum of the resulted cross sections and not just a statistical acceptable number or a specific region of interest.

Objective

In the current study, the longitudinal distribution of histological structures exhibited in the hind limb of a cat (*Felis* sp.) is presented, with an emphasis on Haversian bone. Aiming to preserve the comprehensiveness and consistency of our results, bones (a femur and a tibia) from two different anatomical locations, but in longitudinal continuity were used. Having used the same animal, species and age discrepancies have been eliminated. The objective, of the present research, is to provide the histomorphological and histomorphometrical profile of our samples under the prism of the existing biomechanical regime. In addition, it is examined if intra-skeletal and/or inter-cortical and intra-cortical differences could be associated with strain and load variances experienced individually by each sample. Emphasis is given in providing equally the distribution of bone tissue types and the metrical characteristics of Haversian systems (area and circularity). It is also attempted to present the preliminary observations concerning the *liaison* between OPD and circularity.

Endeavoring to designate and interpret any dispersal differences, the use of GIS was employed, not only as a mean of calculation, but also to statistically and spatially analyze the measured microstructural features. In the current study, the utility of this software is not questioned, on the contrary, it is reinforced, since its selection is established on the fact that it can histologically approach the samples with the best conceivable accuracy. Thus, as a secondary emerging purpose, it is attempted to confirm that histological mapping, though a recently introduced methodology, can and should be applied in histologically related research articles, regardless of discipline or background.

Material and methods

Histological procedure

To realize the present study, the right femur and tibia from the same domestic cat (*Felis* sp.) were examined. The bones originated from the collections of the School of Veterinary Medicine, of the Aristotle University of Thessaloniki (AUTH). The supplied material concerns a single animal with no information about the exact age and sex, but with evident skeletal maturity, confirmed by ossified epiphyses.

After defleshing the bones, the boiling procedure begun, which ensured the removal of any left soft tissues and the adequate degreasing of our samples (Eliopoulos et al. 2007). From each bone, five (5) transverse cross sections were produced. Each cut followed a longitudinal distance of one centimeter (1 cm) from the next, beginning from the proximal and ending at the distal epiphysis. The bone segments were, then, embedded in transparent epoxy resin and consequently subjected to seven (7) sequential polishing stages (*polishing procedure ranged from 90 μm (or 220 grit) up to 1μm*). Prior to the microscopical examination, carbon coating was required. All samples were observed and photographed under Backscattered Electron (BSE) emission mode on a Scanning Electron Microscope (SEM—JEOL JSM-5600 combined with an energy-dispersive microanalysis system—OXFORD LINK ISIS 300—with software ZAF correction analysis). SEM was selected as the mean of observation, because (in BSE mode) it provides images where osteon contours are well recognized (Mears et al. 2015) and it, also, constitutes a direct (but, usually, not quantifiable with EDMS) estimation of osteons mineralization phase (*dark grey osteons are less mineralized and thus younger than those depicted in light-grey color*).

The obtained images were processed using Adobe Photoshop CS5 software, which permitted their high-resolution analysis and accurate assembling, to acquire each whole cross section as a "panorama".

Geographical information systems (GIS)

In the current study, Geographical Information Systems (GIS) are applied to histologically analyze the selected samples. It constitutes a familiar, cost-effective, and user-friendly software, that can perform an in-depth study concerning both the histomorphological appearance and the histomorphometrical estimation of the cortex. The spatial visualization and the consequent spatial analyses of variables are the main reasons behind the choice of this software. This procedure does not constitute an over-simplification of the studied section; on the contrary, it reinforces the most interesting (according to the present research) characteristics and presents them as an entity, in the form of comprehensible and informative maps.

To do so, the assembled complete cross sections were processed via ArcGIS v.10.3 ESRI, to manually digitize all the structures of interest, in previously created shape files. During the preliminary stage of drawing, all indispensable features, such as the periosteal contour and the endosteal contour of each sample, were illustrated. By the time the editing procedure was completed, the initial image could be removed and the resulted map was ready to be acquired. Following the requirements of our study, the focus was, mainly, on the building of polygons that represent the observed Haversian systems and canals. During the editing process, the Haversian systems that were excluded

concerned drifting osteons, multiple canal osteons and, when encountered, primary osteons as products of modeling. Extra attention was given, during drawing, to combine each Haversian canal to its corresponding Haversian system. Area and perimeter were calculated for all the edited features via ArcGIS. Diameter was provided as a mean value, since it was calculated with two manners for each feature. Using the perimeter, diameter is expressed as: diameter = perimeter/π, whereas via area is calculated as: diameter = $\sqrt{(4 \times \text{area})/\pi}$. Approximately 14,500 remodeling features were identified and depicted, from a total of ten transverse cross sections. Despite the fact that our attention was concentrated on Haversian bone, during the histological study of our samples, tissue types of primary periosteal and endosteal origin were also encountered. To provide a holistic view of our material, the creation of additional shape files depicting periosteal lamellar and endosteal bone was also in order (Enlow and Brown 1956; McFarlin et al. 2008).

The emphasis behind the choice of GIS was given to the ability of this software to provide information and not just data. The initial map of each cross section includes all the edited layers of interest. Nevertheless, after the creation and presentation of the shapes, their statistical spatial analysis followed, to highlight the statistically significant structures and to identify their possible distributional patterning. Moving on, two types of analyses were employed. The first analysis was based on Getis and Ord publication (1992), where the employment of *G* statistics provides a safe and direct path to correlate the degree of spatial association within a chosen observation. The resultant *z* scores and *p* values give the spatial clustering of features with both high and low values. In every map, the depicted clusters (high and low) are statistically significant (a feature presents statistical significance, when exhibits high value and it is surrounded by other features (neighbors) with high values, as well. The same applies for low-value features) and present confidence intervals from 90% up to 99%. To comprehend deeper spatial distribution, *G* statistics are usually conjunct with Moran's *I*. Towards this direction, the second analysis was made according to Anselin's research (1995). Anselin proposes the *LISA* (Local Indicators of Spatial Association) statistical analysis, not only to spatially classify the features through *G* statistics, but mainly to identify the spatial outliers, within the resulted clusters. Again, it is clarified that the estimations are only interpreted through the calculations of *z* scores and *p* values. The confidence interval that set statistical significance, in the current method, is 95%. At this point, it is must be emphasized that during Getis—Ord and Moran's analyses, the same clusters of high and low values were identified. Since this was interpreted as confirmation, clustering analysis maps originate from the first methodology, whereas Moran's processing is limited to providing maps depicting only the detected outliers.

The data that were subjected to the aforementioned analyses were osteon and Haversian canal circularities, osteon and Haversian canal areas, as well as their in-between ratio. Moreover, it is clarified that the area of every Haversian system minus the area of its corresponding Haversian canal was also calculated and spatially analyzed (Black et al. 1974). Considering the fact that the results were identical with those of the basic osteon area, solely the last is provided in the following maps.

Adapted from McFarlin (2008) and Gotcha et al. (2016), each bone section was divided into three circumferential rings (inner, middle, and outer) and into eight radial sectors—*octants* (four principle regions: anterior, posterior, medial and lateral, and four derived regions: anterolateral, anteromedial, posterolateral, and posteromedial). These segmentations were employed to produce an oriented quantitative analysis of the spatial distribution of histomorphological structures, by following the guidelines of the reviewed literature. An additional reason was to provide uniformly oriented and divided cross sections to facilitate observation and to permit the comparison between our sections and those of the existing literature, whether they constitute whole or fragmented samples.

Results

Histomorphology

The cortical bone and medullar cavity of femoral and tibial samples are histomorphologically examined. In femoral cross sections, the average percentage of cortical bone is 60%, with the remaining 40% being occupied by the medullar cavity. Tibia presented values of 77% and 33% accordingly. Table 1 provides and combines the results of each histomorphological characteristic for both femoral and tibial cross sections.

Individually, each cross section is maintained as symmetrical as possible and the overall shape is adapted to its anatomical position (proximal–distal). However, it is only appropriate to highlight some tendencies. The performed calculations show that the minimum percent of cortical bone (and consequently the maximum percent of medullar cavity) is ascribed to section e for both the femur and the tibia. The most remodeled sections are e and d for femur and tibia, respectively, since they present the highest percent values of osteonal bone. The least remodeled section is c for both femur and tibia. Concerning the shape of the cross sections, the most circular is c and e for the femur and the tibia accordingly.

To quantify, across every section, the expansion of the basic tissue types, it is calculated the percent of the area that they occupy. The principle tissue types, that are

Table 1 Results of the calculated variables (abbreviations according to Parfitt et al. (1987)) of femoral cross sections along the proximo-distal axis (M stands for the maximum value and m for the minimum)

	Variables					
	Ct.B.Ar (μm^2)	Ct.B.Pm (μm)	Ct.B.Cr (unitless)	Me.Ca.Ar (μm^2)	Me.Ca.Pm (μm)	Me.Ca.Cr (unitless)
Proximal epiphysis						
A						
Femur	32,624,000 (M)	29,387.18	0.7784 (m)	20,896,000	19,554.12	0.6864
Tibia	30,372,000 (M)	25,785.2	0.73 (m)	8,200,000	13,638.81	0.55
B						
Femur	27,244,000	26,093.46	0.8087	16,596,000 (m)	17,697.2	0.6656
Tibia	27,264,000	23,868.9	0.8014	9,088,000	14,538.28	0.54
C						
Femur	25,908,000 (m)	25,422.65	0.8496 (M)	17,812,000	16,332.76	0.8387 (M)
Tibia	29,392,000	24,371.39	0.7752	7,268,000	11,947.66	0.6395 (M)
D						
Femur	28,588,000	26,432	0.8262	17,372,000	22,456.59	0.4327
Tibia	25,920,000 (m)	22,396.35	0.8297	7,216,000 (m)	12,145.16	0.6144
E						
Femur	31,976,000	30,543.43	0.8213	29,024,000 (M)	34,813.82	0.3008 (m)
Tibia	26,148,000	22,919.88	0.8566 (M)	9,680,000 (M)	16,737	0.434 (m)
Distal epiphysis						

	Variables						
	% Ct.B	% Me.Ca	% On.B.Ar	% H.B.Ar	% Es.B.Ar	% Lm.B.Ar	% (rest) Ps.Ar
Proximal epiphysis							
A							
Femur	60.96	39.04	27.13	48.14	28.92	17.6	5.37
Tibia	78.74	21.26	40.94	73.91	21.01	–	5.08
B							
Femur	62.14	37.86	19.86	37.12	15.76	33.36	13.77
Tibia	75	25	37.4	79.09	11.49	–	9.41
C							
Femur	59.26	40.74	19.23 (m)	37.3	12.88	30.15	19.66
Tibia	80.17 (M)	19.83 (m)	31.82 (m)	73.88	14.1	–	12.02
D							
Femur	62.2 (M)	37.8 (m)	25.28	54.67	19.93	19.63	5.78
Tibia	78.22	21.78	42.28 (M)	80.83	11.29	–	7.87
E							
Femur	52.42 (m)	47.58 (M)	27.54 (M)	59.78	22.25	–	17.96
Tibia	72.98 (m)	27.02 (M)	38.48	73.41	22.47	–	4.12
Distal epiphysis							

exhibited in the cortex of the femora, are periosteal lamellar, Haversian (or secondary osteonal), and endosteal bone, whereas in tibias, are encountered the same types, excluding lamellar. Endosteal bone exists in all sections covering the area around the medullar cavity. In the femur, lamellar bone, when present, occupies the region which is situated opposite of endosteal bones' main direction of expansion. Haversian bone covers the rest of the cortex area, which, as the main product of remodeling, tends to replace lamellar bone. Tissue-type maps, created in this study, are provided in Figs. 1 and 2. The used colored scale is similar to the one utilized by McFarlin et al. (2016), in means to facilitate comparison.

OPD

OPD distribution was visualized by GIS. According to Gocha and Agnew (2016), both absolute and relative density maps

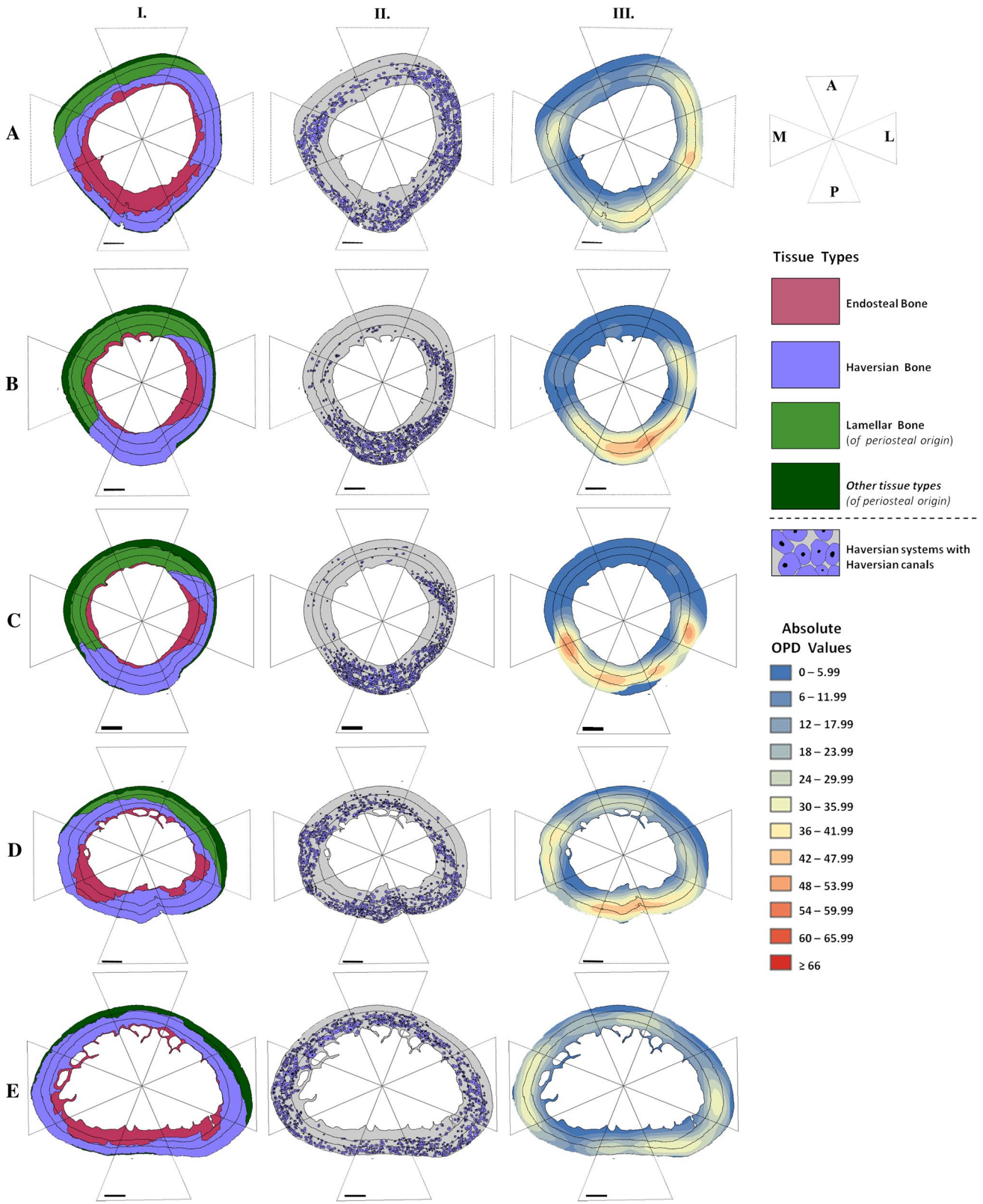

Fig. 1 Femoral histomorphological maps. Every column represents a distinct type of mapping procedure. i.: Tissue-type mapping. ii.: Haversian bone mapping. iii.: Absolute OPD mapping. (Scale bars are equivalent to 1 mm)

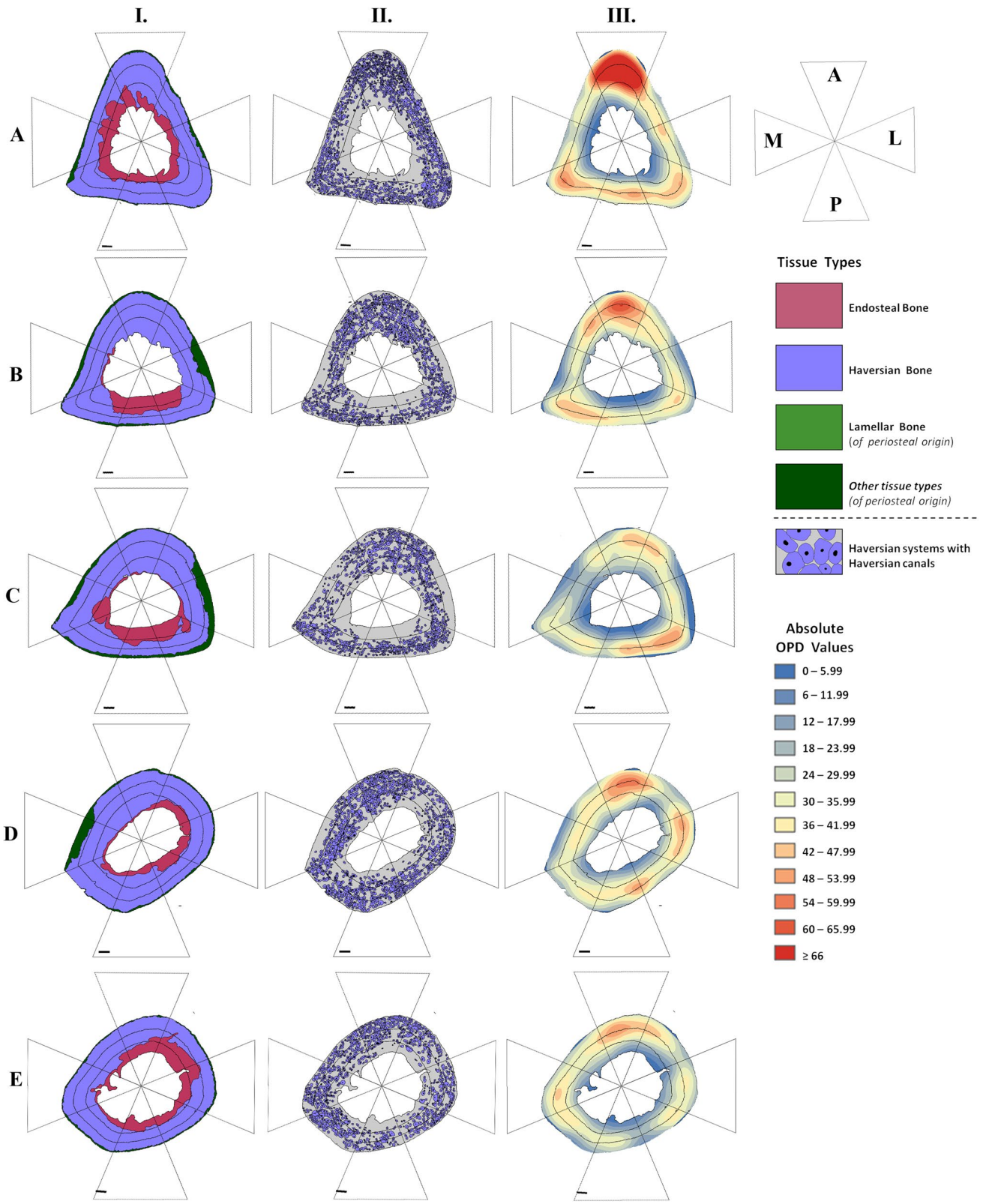

Fig. 2 Tibial histomorphological maps. Every column represents a distinct type of mapping procedure. i.: Tissue-type mapping. ii.: Haversian bone mapping. iii.: Absolute OPD mapping. (Scale bars are equivalent to 1 mm)

were generated. Absolute density maps are presented in Figs. 1 and 2 together with tissue type and Haversian bone maps. Relative density maps are displayed in Figs. 3 and 4 next to circularity maps. This separate arrangement of OPD maps was decided in means to facilitate comparison. Absolute density is not only compared between slices, as cross sections proceed longitudinally, but also, in relation to the spatial distribution of tissue types and mainly Haversian bone. Relative density maps are compared with osteon and Haversian canal circularity maps, because it is important to examine if osteon circularity and OPD distribution are closely related (Britz et al. 2009; Dominguez and Crowder 2012; Keenan et al. 2017).

Absolute OPD

Absolute density takes into consideration both femoral and tibial OPD. Towards this direction, OPD values were divided into 12 classes. The covered range, which was evenly divided among the first 11 classes, was from zero (0) up to 66 remodeling events per square millimeter, whereas the 12th represented values over 66. In Figs. 1 and 2, the absolute density maps for femoral and tibial sections are depicted. Adapted from Gocha and Agnew (2016), a similar colored scale was used to visualize OPD distribution across the section area, with blue to represent the lowest values (lower than 6), while red represented the highest values (over 66). Observations of the femoral slices revealed that sections b and c exhibited the highest OPD values, whereas when tibia was examined the highest values were ascribed anteriorly to sections a and b. Nonetheless, it must be emphasized that the OPD distribution in tibial section b was size restricted compared with section a.

The meticulous examination of both femoral and tibial slices showed that femoral section e exhibited the lowest OPD values, while tibial section a was recognized as the one with the highest and most spatially expanded OPD values.

Relative OPD

Relative OPD expresses the individual OPD that is exhibited in each sample. The same colored scale is used here as well, with the difference that blue color stands for the lowest and red for the highest value presented per sample. Cross sections are not studied as an entity, but separately. Although this type of map provides useful information about the most remodeled cortex area (Gocha and Agnew 2016), the ultimate goal is to investigate any patterns that could possibly connect OPD, mainly, with osteon circularity and secondly with Haversian canal circularity.

Observing Figs. 3 and 4, it is clear that the same areas, that presented the highest absolute OPD values, are depicted in these maps as well. The difference lies in the fact that in relative OPD maps additional regions with significant, per sample, densities are recognized.

In femoral samples, the highest OPD values exhibit an important regional distribution across each section. The only region that presents, along the femur, significant remodeling is the lateral side and its anterior and/or posterior extensions.

Increased OPD values are principally observed at the anterior side of all tibial slices, except from cross section c, where they appear posterolaterally expanded.

Histomorphometry and spatial statistics

Haversian bone constitutes the main focus of the present research. The calculations concerning the histomorphometrical characteristics of Haversian bone from each cross section are displayed in Table 2. Area, perimeter, mean diameter, and circularity were calculated for both osteons and Haversian canals, and their values are presented as the mean ± standard deviation.

Femoral and tibial osteons exhibited similar cumulated mean perimeter and diameter values. The same observation accounts for the mean perimeter and diameter values of Haversian canals. Slight differences are noted in both osteon and Haversian canal cumulated mean area values, that were calculated at 12,053.51 μm^2 and 680.51 μm^2 for the femur, in contrast to 12,384.95 μm^2 and 613.3 μm^2 for the tibia.

The overall shape of osteons and Haversian canals is considered quite circular, equally, for the femur and the tibia.

Circularity under spatial clustering analysis

Circularity constitutes an important characteristic that provides information about the shape of osteons and Haversian canals. High scores confirm that the studied feature is circular (since the circularity of the perfect circle is equal to one). On the other hand, the shape of features with low values can only be interpreted as non-circular or irregular (but not elliptical).

The spatial distribution of circularity for osteons and Haversian canals follows in Figs. 3 and 4. Femur observation shows that its sections (apart from a) share some common distributional trends. Concerning osteons, all slices present high-value clusters in the posteromedial side, while low measurements are mainly situated posteriorly. Obviously, each section presents additional regions with significant circularity values. Sections b and c maintain their similarity and display a cluster of high values anterolaterally. Sections d and e are comparable, not only because they share a common cluster of high osteon circularities posteriorly, but mainly because the distribution of low measurements is similar between osteon and Haversian canals per sample. Section a displays circular osteons anteriorly and Haversian canals anterolaterally. Haversian canal shape irregularities are observed in the lateral and posteromedial side of the cortex.

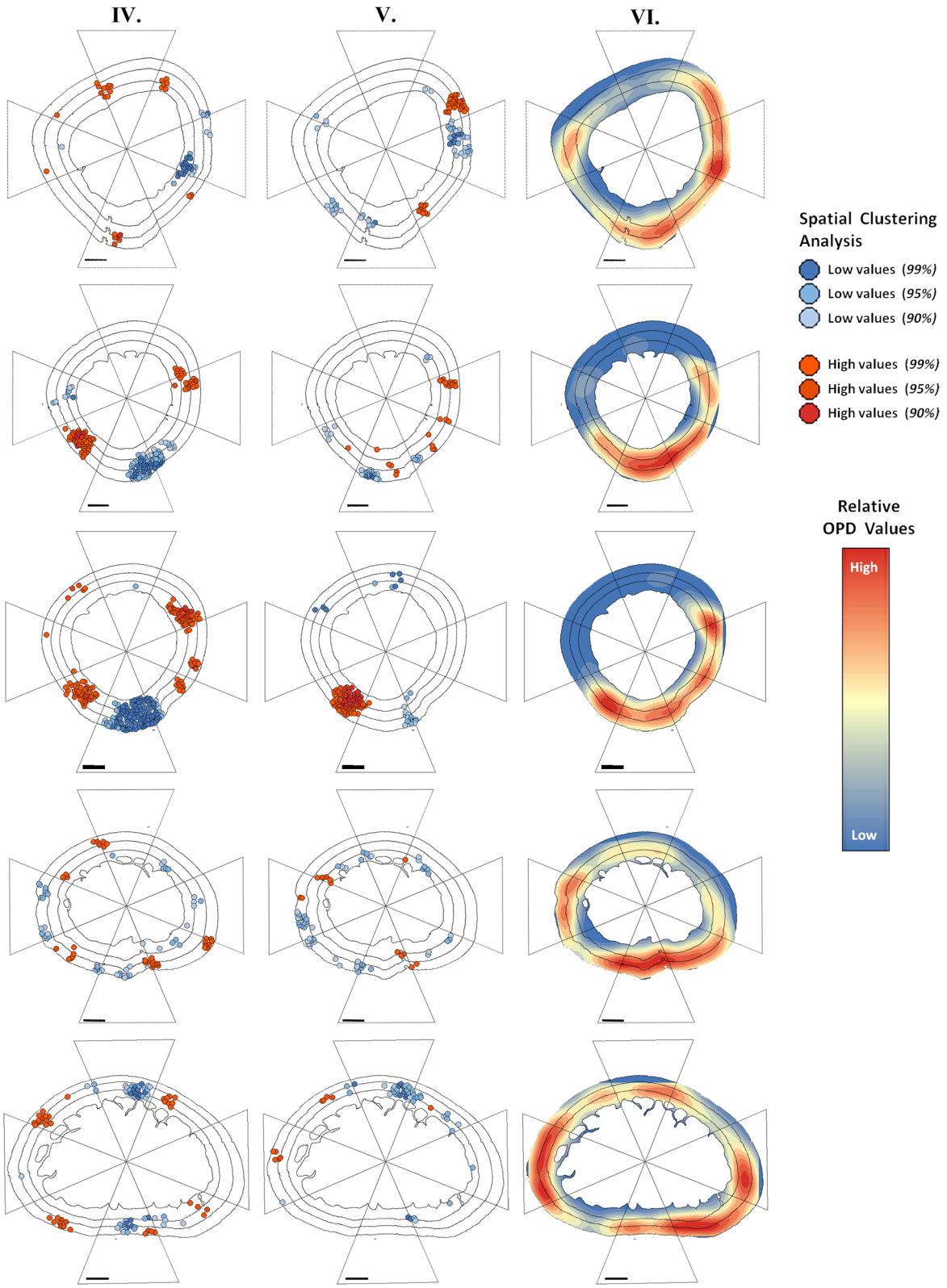

Fig. 3 Femoral histological maps. The depicted spatial clustering analyses are based on: iv.: Osteon circularity and v.: Haversian canal circularity. In means of comparison is provided column vi.: Relative OPD mapping. (Scale bars are equivalent to 1 mm)

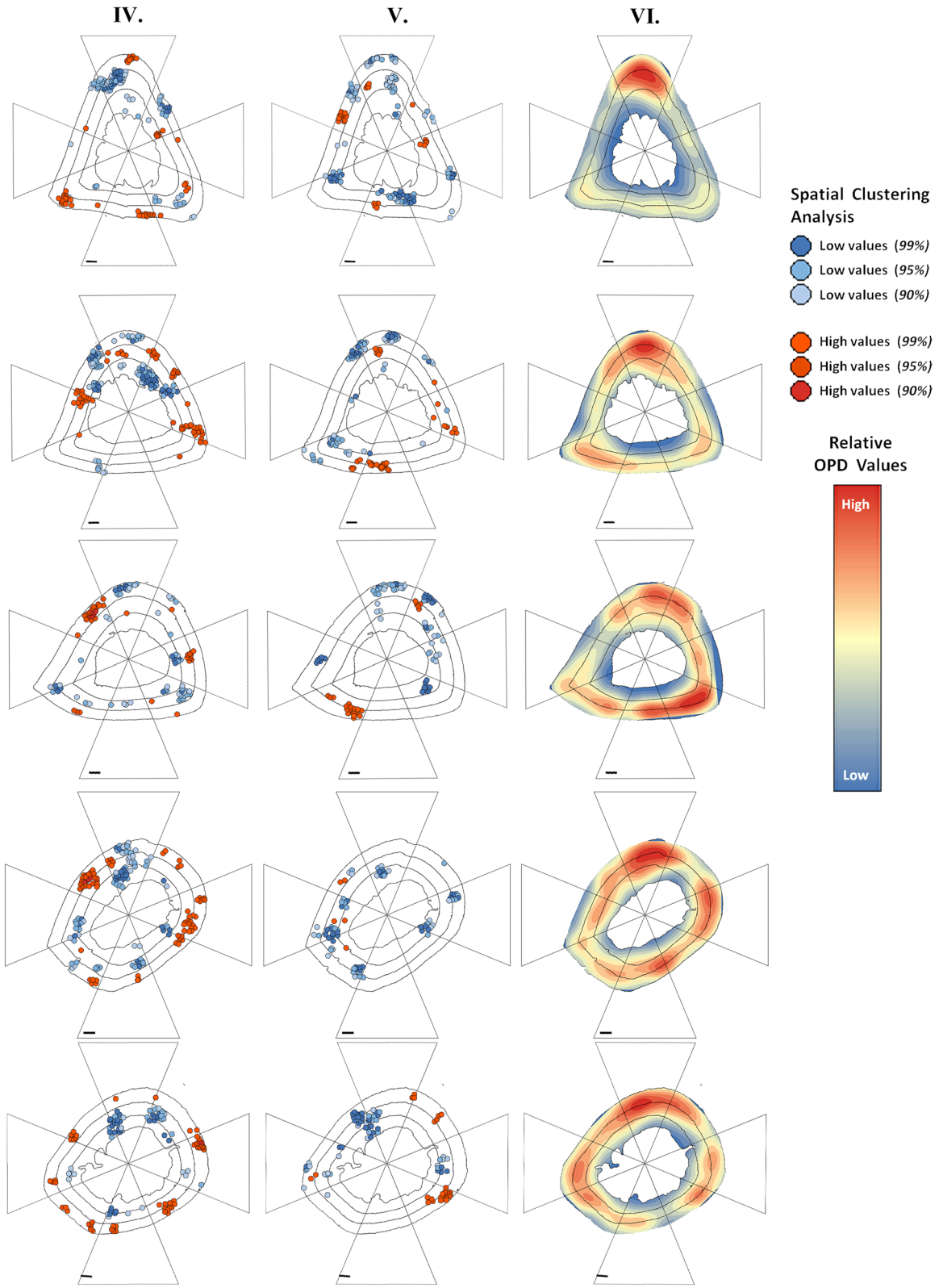

Fig. 4 Tibial histological maps. The depicted spatial clustering analyses are based on: iv.: Osteon circularity and v.: Haversian canal circularity. In means of comparison is provided column vi.: Relative OPD mapping. (Scale bars are equivalent to 1 mm)

Table 2 Results of the calculated histomorphometrical variables (abbreviations according to Parfitt et al. (1987)) of femoral and tibial cross sections (M stands for the maximum value and m for the minimum)

	Variables								
	n	On.Ar (μm^2)	On.Pm (μm)	On.Dm (μm)	On.Cr (Unitless)	H.Ca.Ar (μm^2)	H.Ca.Pm (μm)	H.Ca.Dm (μm)	H.Ca.Cr (Unitless)
Proximal epiphysis									
A									
Femur	633	13,983.36 ± 7969.11 (M)	425.38 ± 123.89	131.88 ± 37.67	0.9059 ± 0.064	547.68 ± 489.52 (m)	79.6 ± 31.86	24.93 ± 9.93	0.9399 ± 0.04
Tibia	1111	11,192.32 ± 7466.15 (m)	373.49 ± 125.19	116.16 ± 38.31	0.9171 ± 0.058	559.37 ± 355.75 (m)	79.17 ± 37.53	24.72 ± 11.51	0.935 ± 0.056 (m)
B									
Femur	486	11,134.76 ± 5908.15	381.31 ± 102.49	118.24 ± 31.33	0.9053 ± 0.06	623.59 ± 387.7	83.31 ± 38.92	26.05 ± 12.07	0.9367 ± 0.042
Tibia	864	11,802.22 ± 7568.57	380.82 ± 126.02	118.89 ± 38.86	0.93 ± 0.051 (M)	605.67 ± 443.85	81.37 ± 39.65	25.45 ± 12.31	0.9358 ± 0.051
C									
Femur	487	10,228.76 ± 7065.76 (m)	361.27 ± 126.93	111.63 ± 38.07	0.8992 ± 0.063 (m)	570.45 ± 381.72	79.48 ± 36.8	24.91 ± 11.43	0.9418 ± 0.039 (M)
Tibia	765	12,223.79 ± 7911.41	389.98 ± 126.8	121.5 ± 38.92	0.924 ± 0.052	616.17 ± 408.66	82.07 ± 39.36	25.71 ± 12.25	0.9411 ± 0.047
D									
Femur	654	11,052.28 ± 6471.46	375.88 ± 108.1	116.83 ± 33.36	0.9121 ± 0.057	663.23 ± 471.32	86.06 ± 42.53	26.8 ± 13.02	0.922 ± 0.056 (m)
Tibia	818	13,396.58 ± 8660.37 (M)	409.66 ± 133.49	127.44 ± 40.79	0.9192 ± 0.057	640.36 ± 588.29	81.81 ± 46.06	25.56 ± 14.12	0.9382 ± 0.054
E									
Femur	635	13,868.38 ± 8828.27	419.28 ± 124.8	130.45 ± 38.44	0.9169 ± 0.582 (M)	997.59 ± 837.91 (M)	104.78 ± 52.59	32.69 ± 16.14	0.9334 ± 0.061
Tibia	756	13,309.83 ± 9444.33	406.51 ± 141.06	126.28 ± 43.32	0.9128 ± 0.061 (m)	644.92 ± 624.79 (M)	83.79 ± 46.65	26.01 ± 14.05	0.947 ± 0.075 (M)
Distal epiphysis									
Femur	Mean:	12,053.51	392.62	121.81	0.9079	680.51	86.65	27.08	0.9348
Tibia		12,384.95	392.1	122.05	0.9206	613.3	81.64	25.49	0.9394

Tibial circularity for both osteons and Haversian canals seems scattered and random. Yet, a thorough observation of Fig. 4 provides certain tendencies. High values are mainly situated in the outer and lesser in the middle rings, whereas the majority of low measurements occupy the middle and inner rings. Section a displays circular osteons posteriorly and posteromedially, while irregular shapes are encountered anteriorly and anterolaterally. Shape irregularities, regarding Haversian canals, are noted, but not limited, to the posterior side. Clusters of high values are observed anteromedially, laterally, and posteriorly. The rest of the cross sections present circular osteons at the anteromedial and lateral sides of the cortex. Low values are mainly, but not solely, situated in the anterior side. Concerning Haversian canal circularity, it seems that the distributional pattern of both high and low values acts supplementary to osteon circularity.

Area under spatial clustering analysis

The spatial distribution of histological characteristics concerning osteon and Haversian canal areas, as well as their in-between ratio, is presented in Figs. 5 and 6.

In femur, section a exhibits the highest osteon area values anterolaterally and medially, whereas the lowest are noted posteriorly and posterolaterally. Haversian canal area exhibits its highest values mainly posteriorly and then laterally, whilst its lowest value is situated medially. Apart from section a, in the rest of the femoral samples, high osteon areas coincide, generally, with high Haversian canal areas, while the same is observed for the lowest values as well. In sections b and c, the highest values are concentrated posteriorly, whereas the lowest are expanded laterally. Similarities are also detected between sections d and e. The highest measurements expand from the medial to the anteromedial side, and the lowest range from the posteromedial up to the posterolateral side. A cluster of high values is noted laterally in section d.

Despite the existence of small divergences, in general, tibial osteon and Haversian canal areas spatially coincide. In section a, high values are coordinated in the anterior and lateral sides of the cortex. Controversially, low measurements of osteon area are concentrated solely in the anterior side, whereas those of Haversian canals appear scattered in the anterior, posteromedial, and posterior sides of the cortex. Sections b and c present similarities, since their high values

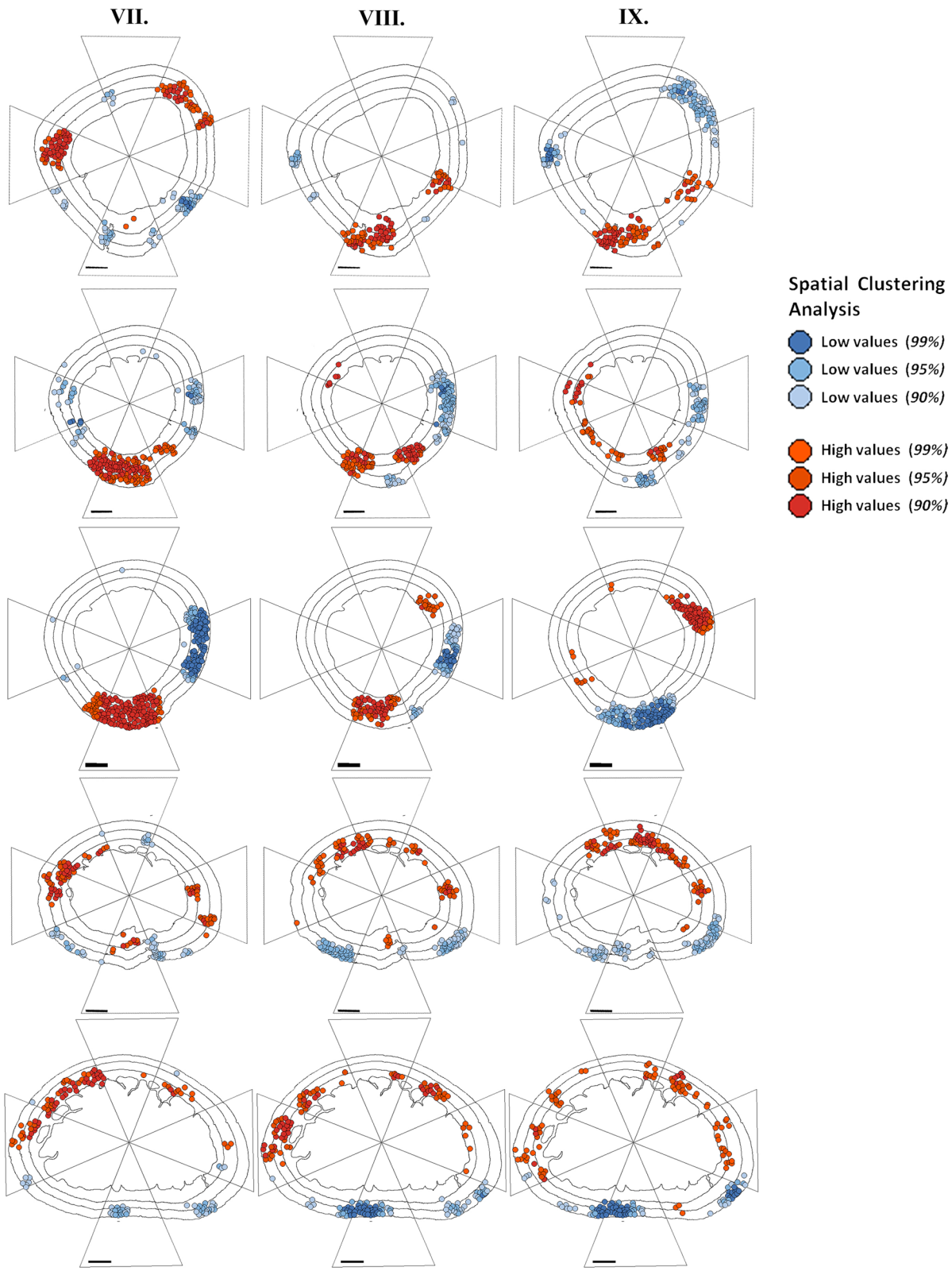

Fig. 5 Femoral histomorphometrical maps. The depicted spatial clustering analyses are based on: vii.: Osteon area. viii.: Haversian canal area. ix.: Percent (%) of each osteon area occupied by its corresponding Haversian canal. (Scale bars are equivalent to 1 mm)

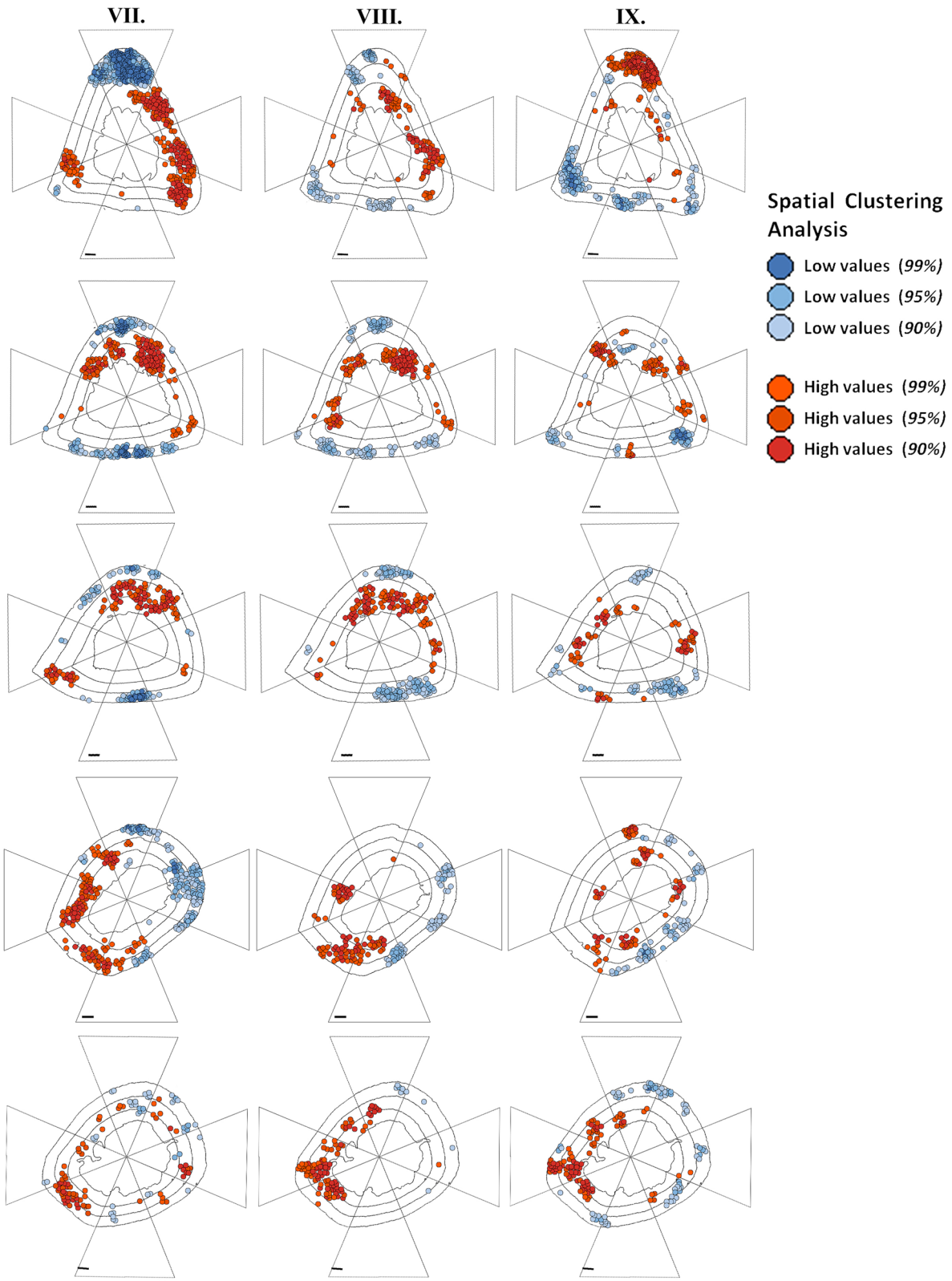

Fig. 6 Tibial histomorphometrical maps. The depicted spatial clustering analyses are based on: vii.: Osteon area. viii.: Haversian canal area. ix.: Percent (%) of each osteon area occupied by its corresponding Haversian canal. (Scale bars are equivalent to 1 mm)

are concentrated in the anterior side, with slight expansions both anteromedially and anterolaterally. Low measurements are situated in the periphery of the cortex (outer ring), mainly, anteriorly and posteriorly. Sections d and e appear rather equivalent concerning high measurements, since they present them in the posteromedial and medial side of the cortex. Regarding low values, they are observed laterally and posteriorly in the fourth section, while in the fifth, they are hardly noted.

The additional characteristic that was spatially analyzed was the percent of each osteon area occupied by its analogous Haversian canal. In the femoral sections, the distribution of high values does not follow an obvious pattern. The only apparent trend was that they followed (excluding section c) the distribution of the increased Haversian canal area values, which is also encountered in tibial section e. The lower values are mainly situated posteriorly, with the exception of section a, where their distribution is presented anterolaterally and anteromedially. Observations of the tibial sections revealed that high values do not present a distinct distributional pattern longitudinally, since they are situated in different cortex regions in each section. A general remark (excluding section d) is that these measurements are noted in the opposite direction to the main endosteal bone expansion. Low values are mainly, but not exclusively, located posterolaterally and posteriorly. Each section may present additional low-value clusters to other cortex regions, as well (for example, section a presents a robust cluster posteromedially).

Area and circularity under spatial outliers' analysis

Focusing on the results derived from spatial outliers' analysis for both area and circularity, no discernible patterns are encountered. The only observation about femoral cross sections is that the majority of outliers, either of high or low values, present a linear spatial distribution amongst them. Apparent groups of outliers are rarely noted and they are limited to sections b and d ("Appendix", Fig. 7).

Instead, the noted distribution of the corresponding tibial characteristics appears rather random and scattered. Contradicted with femoral slices, tibial cross sections seldom present accumulated registrations or linear relations among outliers. Nonetheless, it is observed that the first section is the most populated concerning the detected outliers ("Appendix", Fig. 8).

Discussion

Bone histomorphology

The diversity of bone tissue types is apparent in the present study and expresses intra-skeletal variability. Regarding femoral cross sections, lamellar bone is exhibited in four out of five slices. As above-mentioned, when present, this tissue type occupies the area opposite from endosteal bone. The rest of the cortex area is covered by Haversian bone, which exhibits its highest OPD values in the opposite direction to the lamellar bone expansion. On the other hand, in the fifth femoral cross section and in the entity of tibial cortex, only Haversian and endosteal tissue types are noted. Despite the fact that the tibia presents significant differences in the cortical bone area longitudinally, the overall distribution of tissue types exhibits greater uniformity than in the femur. Allen and Burr (2014) stated that, during the longitudinal growth of bone, modeling resorption removes bone from the periosteal surface, while in the meantime, novel bone is deposited on the analogous endosteal surface by modeling formation. For the maintenance of the bones' equilibrium, Enlow (1962a, b) suggested that, during regional changes in shape, when tissue is added on the periosteal surface, sequentially, the other side experiences resorption. Both these mechanisms can be used for interpreting the aforementioned distribution of tissue types, but this conflicts with the anticipated reduction of the modeling process in an adult animal. The answer sources from Lieberman et al. (2001, 2003). In their research, they corroborated that bones of the hind limb respond, via modeling and remodeling, differently to the increased loading regime implemented along the proximo-distal axis. Specifically, it is stated that periosteal bone addition characterizes segments closer to the proximal epiphysis, whereas distal samples displayed higher remodeling rates. Although their results were based on quadrupedal cursorial animals, our study confirms the aforementioned observations for *Felis* sp., which appertains to the category of quadrupedal digitigrade animals. More thoroughly, the first cross sections for both femur and tibia exhibit the highest compact bone areas, and thus, the opinion, that bones closer to proximal epiphyses adapt to strain forces by augmenting their mass constraint, is verified. Furthermore, all tibial sections and the fifth femoral, presented the greatest Haversian bone portions, a fact which confirms the elevated remodeling rates exhibited in the distal segments (Drapeau and Streeter 2006; Lieberman and Crompton 1998).

Observing the corpus of all above-mentioned histomorphological characteristics, certain similarities become apparent. Concerning the femur, the most similar cross sections are b and c, whereas, when observing, the tibia, resemblances exist among slice b and c, and also between d and e. Similarities between neighboring cross sections are anticipated, since they might be experiencing analogous mechanical loading with resemblances in the distributional pattern. These similarities, or the corresponding differences, that are presented inter-cortically, are expressed and sometimes can define the distribution of the studied histomorphometrical features. Thus, it is rather unlikely for a given feature (e.g.,

OPD) to be completely independent from the effective biomechanical regime.

Although modeling escapes from the objectives of the current study, we ought to mention the following observation. Without exception, all ten sections presented endosteal bone, which appears to present a counter-clockwise rotation. If excessively, we take a leap and associate this tissue type with what is known as endosteal lamellar pocket (ELP), then certain tendencies are noted (Maggiano et al. 2011). ELP constitutes a histomorphological meta-feature that has been used as a directional indicator of modeling drift, although it is known that drift varies in direction and magnitude along the diaphyses. As observed here, the highest area values of endosteal bone are attributed to the four slices closest to the proximal and distal extremes of both femur and tibia (Maggiano 2012; Maggiano et al. 2015). Supplementarily, endosteal bone distribution of each slice could be considered as a precursor of the geometrical changes found in the shape of the following section (Goldman et al. 2009). Therefore, it must be emphasized that endosteum is not only osteogenic, but dynamic, since it plays a determinant role during the modeling process, by contributing to the shaping of the diaphyseal curvature, diameter, and the overall position of bone.

Circularity and OPD

Circularity calculations often serve in approaching, and when possible answering, queries regarding species differentiation, aging, and also mechanical adaptation of bone. Numerous studies tried to distinguish animal from human bones via circularity measurements and have concluded differently (Crescimanno and Stout 2012; Dominguez and Crowder 2012; Tersigni-Tarrant et al. 2011). OPD, on the other hand, is a method, usually followed when considering ontogenetical trend or its derivative estimation of age-at-death (Frost 1987b). After all, increased remodeling densities are associated with cortex regions that experiencing higher effective age (Gocha and Agnew 2016; McFarlin et al. 2008).

In Table 2, it is presented the diversity experiencing osteon circularity equally among cross sections of the same bone and between bones from two different anatomical positions. A general observation is that neither femoral nor tibial slices present OPD values at the endosteal third ring of cross sections. In addition, in femoral section c, increased OPD values are situated anterolaterally and posteriorly. The anterolateral expansion of high OPDs was primarily commented by Gocha and Agnew (2016), who in their study of the human femora, connected it, among other reasons, to strain environment and to a relevant with obligate bipedalism mechanical loading. Nonetheless, as it results from our observations, increased OPD values, in the anterolateral region, are also encountered in quadrupedal animals, as well.

According to Keenan et al. (and references therein) (2017), the femur exhibits a moderate-complexity status, excluding its mid-shaft which along with the tibia appertain to a high complexity load category. As it is stated in the same study, high complexity bones tend to present lower average osteon circularities than moderate. This is in accordance with the minimum value that is observed in femur section c (0.8992), but it is contradicted with the rest of the measurements, since the tibia displays greater circularities than the femur. This, exhorts us to consider that load positively affects the average circularity within the same organism. Regarding Haversian canal circularity, it displays a homogeneity between bones, as well as between sections.

A tendency that is noted, by simultaneously observing circularity and OPD maps, is that the majority of irregular shapes (low circularity) are situated near areas exhibiting high OPD values, with the unique exception of the femoral cross section c. On the other hand, circular features are usually encountered in areas presenting more moderate OPD values. Perhaps, high OPDs tend to affect osteon shape, since their accumulation can potentially alter their circularity, either by compressing them or by turning them into fragments due to the formation of the next osteon generation. Albeit, providing conclusions in a deterministic manner is not attempted. We ought to consider that our results were not aligned with the anticipated outcome according to Britz et al. (2009) and Domingeuz et al. (2012) and to respect the opinion of Keenan et al (2017), that habitual load environment is not apparent in circularity values. Nevertheless, we support our observations and we vigorously advise that further research should test the existence of a threshold, above which circularity becomes gradually more irregular, due to osteon overpopulation and/or the coexistence of different osteon generations. Maggiano et al. (2017) documented what affects osteon circularity, but the reasons that cause or initiate these circularity fluctuations remain to be unveiled.

Finally, the results derived from spatial outliers analysis were not conclusive for both area and circularity examination. Even when considering that some outliers could forebode the clusters of the following section, this notion was limited to femoral section a and c. Distinct patterns were not recognized and those that hinted linear or accumulating relations, could be attributed neither to targeted, nor to stochastic remodeling.

Bone histomorphometry

Haversian systems (also referred to as osteons) are the main structures of cortical bone, and constitute the basic product of bone remodeling. Having focused the present study on them, it is evident that bone it is not static, but aims to be homeostatic. In each cross section, osteon and Haversian canal areas present a uniformity in their distributional pattern (except from

femoral slice a). These concentrated clusters of high and low area values tend to be interpreted in means of mechanical loading. Without excluding stochastic (non-targeted) remodeling, regions exhibiting large osteon and Haversian canal areas are most likely experiencing lower strain magnitudes, that are in accordance with tension mode. Focusing on femoral cross sections b and c, wider features are situated mainly in the posterior side of the cortex. As it is known, this is the location of *linea aspera*, where muscular exertion is placed, and consequently, it is considered as a region with evident tensile stress (Barbos et al. 1983). From femoral sections d and e, up to the most distal tibial sample, high values of osteon and Haversian canal areas are mainly situated oppositely of the principal direction of endosteal bone expansion, in the middle and inner ring of the cortex. On the contrary, the lowest area values are considered as indicators of compression *milieu*. They are usually situated periosteally, mainly, occupying the outer ring of the cortex, where the strain environment is tense (Frost 1990). The above-mentioned inverse relation between osteon size and strain environment has also been confirmed by numerous studies (Frost 1990; Skedros et al. 1994, 1997; van Oers et al. 2008). Undoubtedly, smaller osteons improve the response of bone to mechanical load. Small-sized osteons tend to augment the fracture toughness and ameliorate the overall fatigue properties of bone (Gibson et al. 2006; O'Brien et al. 2005). The consequent increased spatial osteon density reduces microcrack propagation and enhances pullout resistance (Skedros et al. 2007). Another possible advantage is that, during remodeling, the smaller the resorption cavities formed, the lesser cortex robustness will be affected (Britz et al. 2009). The different distributional patterning of histomorphometrical characteristics encountered intra-skeletally is in consistence with the dissimilarities in strain modes, magnitudes, and in general, stain regimes exhibited among regions of the same bone. It is appropriate to clarify, that, when encountered, microcracks should be examined carefully, to avoid their misclassification as expressions of the existing load regime. As it known, their origin can vary, depending on life-history traits, environmental influence, fatigue, post-mortem reasons, or even on the handling process of skeletal remains during laboratory preparation (Mallouchou et al. 2019).

The ratio between Haversian canal and osteon was calculated to observe the status of osteons' lifetime, and thus conclude upon the phase of the remodeling. High percentages demonstrate still forming osteons, which is equivalent to an active remodeling cycle. The rest of the osteons either go through the mineralization phase, or they are characterized by the stage of quiescence (resting) (Allen and Burr 2014). The majority of areas exhibiting active formation coincide with regions presenting high osteon and Haversian canal area values, except from femoral section c and tibial section a. Furthermore, these two sections are the only that, in a comparison between the examined ratio and relative OPD, exhibit their highest values at the same region. The remaining femoral and tibial sections present their highest values at different regions. It is not known if the ratio between Haversian canal and osteon can be used as a potential precursor of the regions, that will develop increased OPDs on the basis of age maturity. Future analyses need to test this possibility, which is quite difficult, especially, because in vivo histological examination of bone growth, maturity, and response of the same individual is not yet possible. After all, one of the main future directives is to escape from a mere investigation of the resulted bone morphology, but to be able to decipher how this morphology was achieved.

In addition, we ought to accept that the plurality of porous spaces are osteon central canals, according to Skedros et al. (1994). Towards this direction, if we regard Haversian canals as pores, then it is demonstrated that the tension cortex exhibits a higher porosity than the opposing compression region. This observation is also in consistence with the inverse relation between porosity, compressive strength, and elastic modulus that was encountered by Carter and Hayes (1977).

Conclusions

In conclusion, it must be emphasized that the studied products of cortical bone remodeling and the underline biomechanical stress operate in a mutual manner. The applied histomorphological and histomorphometrical analyses, as foretold, confirmed that the distribution of the examined microstructural features is defined and defines mechanical loading. Without disregarding the value of non-targeted remodeling, its non-location-specific nature renders it into a cause yet to be more thoroughly determined. Thus, it is only proper to associate the majority of the observed intra-skeletal, inter-cortical, and intra-cortical differences to an analogous spatially distributed pattern of biomechanical regime. Apparently, our efforts were devoted in unfolding the principles that govern histological appearance; nevertheless, potentially, there are still tendencies to be recognized and mentioned, but, for now, remain hidden from our knowledge spectrum. It is envisaged that future research will reveal them and attribute them accurately. Towards this direction, a thorough analysis of each sample is suggested, although, acknowledging the time-consuming character of this type of research. When possible and to conclude safely, we urge the measurement of the full spectrum of the encountered Haversian systems (or any other chosen microstructural characteristic) and not just a statistically acceptable number.

GIS escapes from being considered as a simple processing method; instead, it is strongly recommended as a mean of editing, analyzing and presenting the data of the majority of histological studies. Primordially, it provides an instant

feedback of the exact location of features and of their statistically significant spatial distribution. Despite following a challenging approach via GIS, the results render this software into an indispensable tool for histological mapping and applicable in the examination of all bones, regardless of anatomical position, state of preservation, or represented organism.

In addition, as derived from our results, skeletal fragments, although used universally, do not constitute the best possible representatives of the examined cortex, and much less of the studied bone. To obtain credible results and to contribute to the progress of modern bone histology, the acquisition of complete cross sections, if feasible, is advised. Ideally, along the proximo-distal axis of bone, at least three cross sections (two near the epiphyses and one at the midshaft) could provide not only a holistic microstructural approach, but, mainly, a meticulous examination of bone histology under the prism of its macroscopical position and function.

Although it is acknowledged that our sample size is restricted, this fact did neither impeded the fulfillment of our objectives, nor compromised our results. Notwithstanding, this research constitutes the fundamental first step before conducting any type of comparative study. In our forthcoming studies, the sample size will be substantially increased, to be able to project our observations to the sum of mammalian bones. Undoubtedly, bone histology is the core of various sciences of medical, biological, zoological, veterinarian, forensic, archaeological, and palaeontological provenance. Every new study, which embraces the suggested methodology, is considered as a step of advancement in unveiling the hidden processes of bone organization and growth. By the time bone development is profoundly understood, the majority of histological divergences will be better explored, classified, and then attributed to pathology and/or to other underlying reasons. Thus, the creation of a universal handling and processing method, which eventually will lead to the construction of a histological depository and therefore a database, remains the ultimate goal.

Acknowledgements The authors are grateful to Professor Papadopoulos George for his generosity and for willingly allowing the initial preparation of our samples to be held at the Laboratory of Anatomy, Histology and Embryology, at the School of Veterinary Medicine (AUTH). Assistant Professor Roussiakis Socrates is acknowledged for his valuable encouragement during this research. Emeritus professor Theodorou George is thanked for morally supporting the preliminary steps of this endeavour. The Department of Historical Geology and Palaeontology (UOA) is appreciated for permitting the authors to conduct the histological preparation of the samples at the homonymous laboratory. The Department of Economic Geology and Geochemistry (UOA) is thanked for permitting the authors to examine the samples with SEM.

Compliance with ethical standards

Conflict of interest The authors declare that they have no conflict of interest.

Appendix

See Figs. 7 and 8.

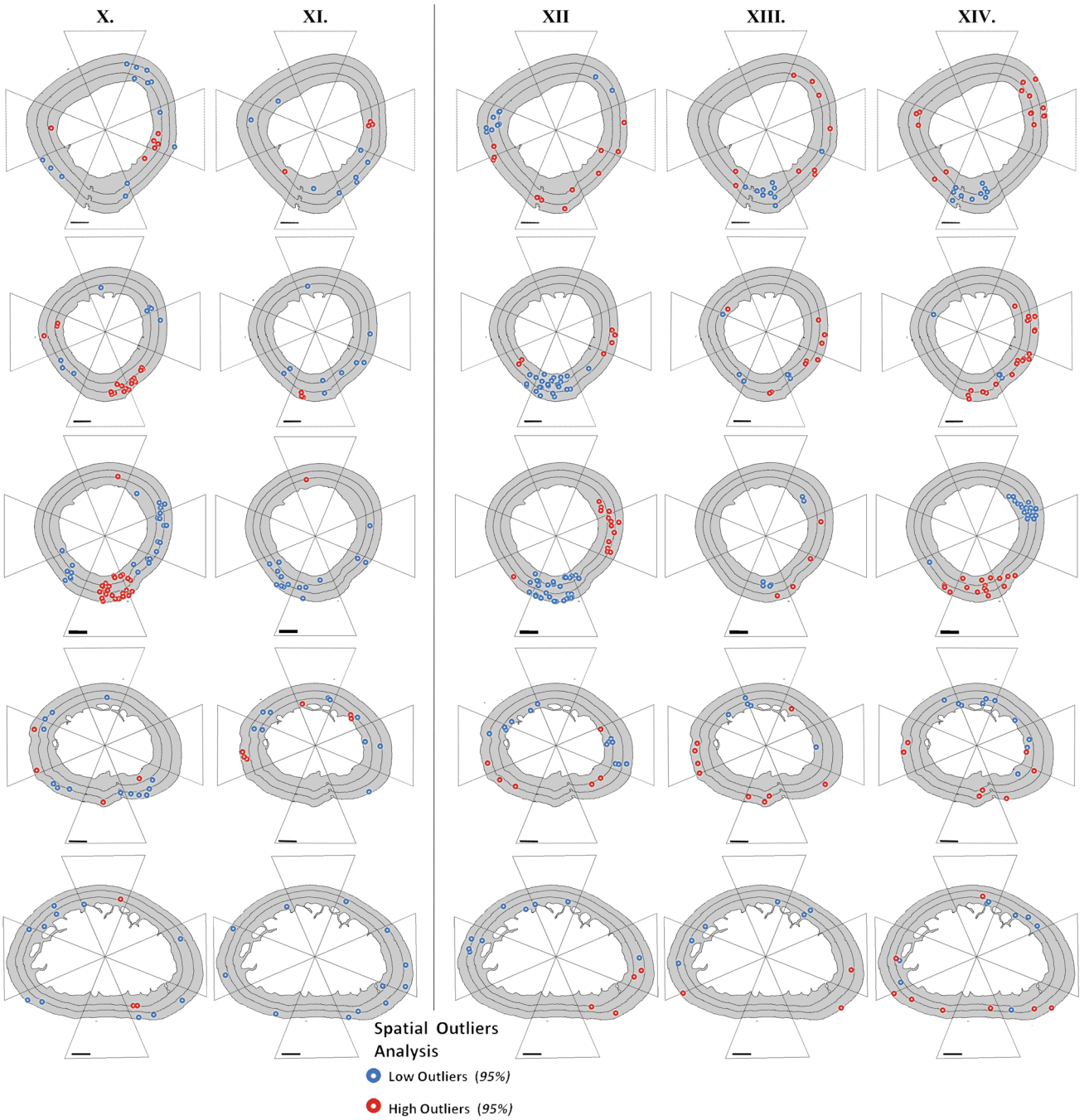

Fig. 7 Femoral histomorphometrical maps. The depicted spatial outliers analyses are based on: x.: Osteon circularity. xi.: Haversian canal circularity. xii.: Osteon area. xiii.: Haversian canal area. xiv.: Percent (%) of each osteon area occupied by its corresponding Haversian canal. (Scale bars are equivalent to *1 mm*)

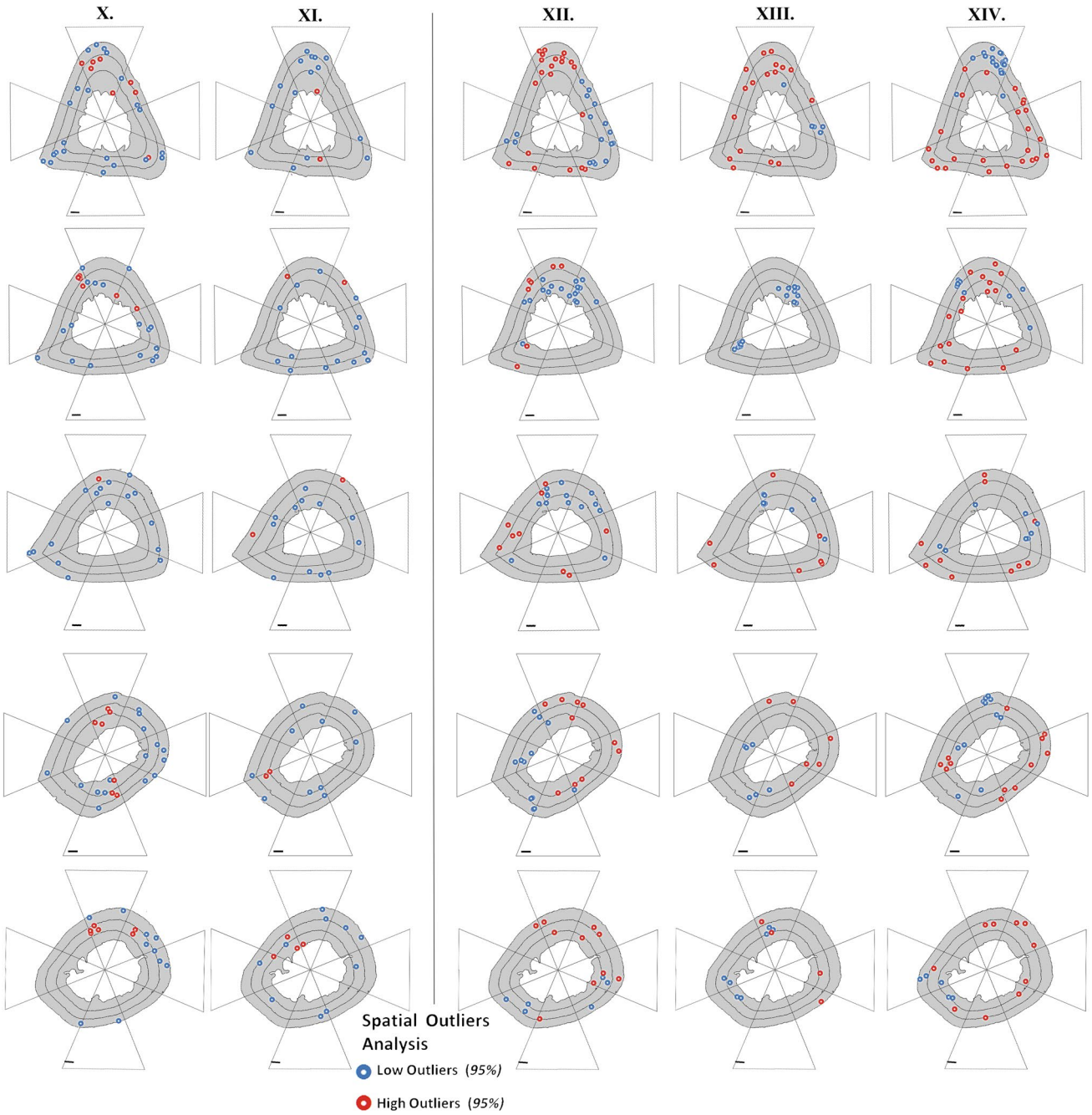

Fig. 8 Tibial histomorphometrical maps. The depicted spatial outliers analyses are based on: x.: Osteon circularity. xi.: Haversian canal circularity. xii.: Osteon area. xiii.: Haversian canal area. xiv.: Percent (%) of each osteon area occupied by its corresponding Haversian canal. (Scale bars are equivalent to 1 mm)

References

Abbott S, Trinkaus E, Burr D (1996) Dynamic bone remodeling in later Pleistocene fossil hominids. Am J Phys Anthropol 99:585–601

Allen M, Burr D (2014) Bone modeling and remodeling. Basic and applied bone biology, pp 75–90

Amprino R (1947) La structure du tissu osseux envisagée comme expression de différences dans la vitesse de l'accroissement. Archives de biologie 58:317–330

Amprino R, Godina G (1947) La struttura delle ossa nei vertebrati: ricerche comparative negli anfibi e negli amnioti.

Anselin L (1995) Local indicators of spatial association-LISA. Geogr Anal 27:93–115

Barbos M, Bianco P, Ascenzi A (1983) Distribution of osteonic and interstitial components in the human femoral shaft with reference to structure, calcification and mechanical properties. Cells Tissues Organs 115:178–186

Black J, Mattson R, Korostoff E (1974) Haversian Osteons: size, distribution, internal structure, and orientation. J Biomed Mater Res 8:299–319

Britz H, Thomas C, Clement J, Cooper D (2009) The relation of femoral osteon geometry to age, sex, height and weight. Bone 45:77–83

Cambra-Moo O, Meneses C, Barbero M, Gil O, Pérez J, Rello-Varona S, Martín M, Martín A (2012) Mapping human long bone compartmentalisation during ontogeny: a new methodological approach. J Struct Biol 178:338–349

Carter D, Hayes W (1977) The compressive behavior of bone as a two-phase porous structure. J Bone Joint Surg 59A:954–962

Cattaneo C, Porta D, Gibelli D, Gamba C (2009) Histological determination of the human origin of bone fragments. J Forensic Sci 54:531–533

Crescimanno A, Stout S (2012) Differentiating fragmented human and nonhuman long bone using osteon circularity. J Forensic Sci 57:287–294

Currey J (2002) Bones: structure and mechanics. Princeton University Press, Princeton, NJ

Diaz C, Rajtova V (1975) Comparative study of lamellar bone in some Carnivora. Folia Morphol 23:221

Dominguez V, Crowder C (2012) The utility of osteon shape and circularity for differentiating human and non-human haversian bone. Am J Phys Anthropol 149:84–91

Drapeau M, Streeter M (2006) Modeling and remodeling responses to normal loading in the human lower limb. Ame J Phys Anthropol 129:403–409

Eliopoulos C, Lagia A, Manolis S (2007) A modern, documented human skeletal collection from Greece. Homo-J Compar Human Biol 58:221–228

Enlow D (1962a) A study of the postnatal growth and remodeling of bone. Am J Anat 110:79–101

Enlow D (1962b) Functions of the Haversian system. Am J Anat 110:269–305

Enlow D (1963) Principles of bone remodeling. Charles C. Thomas, Springfield, IL

Enlow D, Brown S (1956) A comparative histological study of fossil and recent bone tissues. Part I Texas J Sci 8:405–412

Enlow D, Brown S (1958) A comparative histological study of fossil and recent bone tissues. Part III Texas J Sci 10:212–217

Felder A, Phillips C, Cornish H, Cooke M, Hutchinson J, Doube M (2017) Secondary osteons scale allometrically in mammalian humerus and femur. R Soc Open Sci 4

Foote J (1916) A contribution to the comparative histology of the femur. Smithsonian institution. 35.

Frost H (1987a) Bone "mass" and the "mechanostat": a proposal. Anat Rec 219:1–9

Frost H (1987b) Secondary osteon populations: an algorithm for determining mean tissue age. Yearb Phys Anthropol 30:221–238

Frost H (1990) Skeletal structural adaptations to mechanical usage (SATMU): 2. Redefining Wolff's Law: the remodeling problem. Anat Rec 226:414–422

Frost H (1998) Changing concepts in skeletal physiology: Wolff's Law, the Mechanostat, and the "Utah Paradigm". Am J Hum Biol 10:599–605

Getis A, Ord JK (1992) The analysis of spatial association by use of distance statistics. Geogr Anal 24

Gibson V, Stover S, Gibeling J, Hazelwood S, Martin R (2006) Osteonal effects on elastic modulus and fatigue life in equine bone. J Biomech 39:217–225

Gocha T, Agnew A (2016) Spatial variation in osteon population density at the human femoral midshaft: histomorphometric adaptations to habitual load environment. J Anat 228:733–745

Goldman H, McFarlin S, Cooper D, Thomas C, Clement J (2009) Ontogenetic patterning of cortical bone microstructure and geometry at the human mid-shaft femur. Anat Rec 292:24–64

Goliath J, Stewart M, Stout S (2016) Variation in osteon histomorphometrics and their impact on age-at-death estimation in older individuals. Forensic Sci Int 262:282.e1–282e6

Harsanyi L (1993) Differential diagnosis of human and animal bone. In: Grupe G, Garland A (eds) Histology of ancient human bone: methods and diagnosis. Proceedings of the Palaeohistopathology Workshop; October 3–5, 1990, Gottingten, Germany., Springer, London, pp 79–94

Havers C (1691) Osteologia nova, or, some new observations of the bones and the parts belonging to them, with the manner of their accretion, and nutrition.University Microfilms International, Ann Arbor

Hillier M, Bell L (2007) Differentiating human bone from animal bone: a review of histological methods. J Forensic Sci 52:249–263. https://doi.org/10.1111/j.1556-4029.2006.00368.x

Jaffe H (1929) The structure of bone: with particular reference to its fibrillar nature and the relation of function to internal architecture. Arch Surg 19:24–52

Jowsey J (1966) Studies of Haversian systems in man and some animals. J Anat 100:857–864

Keenan K, Mears C, Skedros J (2017) Utility of osteon circularity for determining species and interpreting load history in primates and nonprimates. Am J Phys Anthropol 162:657–681

Kerley E (1965) The microscopic determination of age in human bone. Am J Phys Anthropol 23:149–164

Kumar N, Dantzig J, Jasiuk I, Robling A, Turner C (2010) Numerical modeling of long bone adaptation due to mechanical loading: correlation with experiments. Ann Biomed Eng 38:594–604

Lieberman D, Crompton A (1998) Responses of bone to stress: constraints on symmorphosis. In: Webel E et al (eds) Principles of animal design: the optimization and symmorphosis debate. Cambridge University Press, Cambridge, pp 78–86

Lieberman D, Pearson O (2001) Trade-off between modeling and remodeling responses to loading in the mammalian limb. Bull Mus Comp Zool 156:269–282

Lieberman D, Pearson O, Polk J, Demes B, Crompton A (2003) Optimization of bone growth and remodeling in response to loading in tapered mammalian limbs. J Exp Biol 206:3125–3138

Maggiano C (2012) Making the mold: a microstructural perspective on bone modeling during growth and mechanical adaptation. In: Stout S, Crowder C (eds) Hard tissue histology: an anthropological perspective. CRC Press, Boca Raton, pp 45–90

Maggiano I, Maggiano C, Tiesler V, Chi-Keb J, Stout S (2015) Drifting diaphyses: asymmetry in diametric growth and adaptation along the humeral and femoral length. Anat Rec 298:1689–1699

Maggiano I, Maggiano C, Clement J, Thomas D, Cooper D (2017) Longitudinal variation of osteon circularity in three-dimensional reconstructions of Haversian networks. Am J Phys Anthropol 162:273

Maggiano I, Maggiano C, Tiesler V, Kierdorf H, Stout S, Schultz M (2011) A distinct region of microarchitectural variation in femoral compact bone: histomorphology of the endosteal lamellar pocket. Int J Osteoarch 21:743–750

Mallouchou M, Stathopoulou E, Theodorou G (2019) How do fossilized mammalian bones behave during chemical conservation? The histological case studies of Tilos and Kerassia. Geoheritage 11:597–614. https://doi.org/10.1007/s12371-018-0310-3

Martin R, Burr D, Sharkey N (1998) Skeletal tissue mechanics. Springer, New York

Martiniakova M, Grosskopf B, Omelka R, Vondrakova M, Bauerova M (2006) Differences among species in compact bone tissue microstructure of mammalian skeleton: use of a discriminant function analysis for species identification. J Forensic Sci 51:1235–1239. https://doi.org/10.1111/j.1556-4029.2006.00260.x

Mason M, Skedros J, Bloebaum R (1995) Evidence of strain-mode-related cortical adaptation in the diaphysis of the horse radius. Bone 17:229–237

McFarlin S, Terranova C, Zihlman A, Bromage T (2016) Primary bone microanatomy records developmental aspects of life history in catarrhine primates. J Hum Evol 92:60–79

McFarlin S, Terranova C, Zihlman A, Enlow D, Bromage T (2008) Regional variability in secondary remodeling within long bone cortices of catarrhine primates: the influence of bone growth history. J Anat 213:308–324

Mears C, Litton S, Phippen C, Langston T, Keenan K, Skedros J (2015) Improving accuracy, precision, and efficiency in analysis of osteon cross-sectional shape. Am J Phys Anthropol 156:223

Mescher A (2013) Junqueira's basic histology text and atlas. Mc Graw Hill Education, Medical

O'Brien F, Taylor D, Clive Lee T (2005) The effect of bone microstructure on the initiation and growth of microcracks. J Orthop Res 23:475–480

Parfitt A, Drezner M, Glorieux F, Kanis J, Malluche H, Meunier P, Ott S, Recker R (1987) Bone histomorphometry: standardization of nomenclature, symbols, and units: report of the ASBMR histomorphometry nomenclature committee. J Bone Miner Res 2:595–610

Pfeiffer S, Crowder C, Harrington L, Brown M (2006) Secondary osteon and Haversian canal dimensions as behavioral indicators. Am J Phys Anthropol 131:460–468

Quekett J. (1855) Structure of the skeleton of vertebrate animals. Descriptive and illustrated catalogue of the histological series contained in the Museum of the Royal College of Surgeons of England, R. and J.E. Taylor, London.

Reznikov N, Shahar R, S W. (2014) Bone hierarchical structure in three dimensions. Acta Biomater 10:3815–3826

Robling A, Stout S (2003) Histomorphology, geometry, and mechanical loading in past populations. Bone Loss and Osteoporosis, Springer, pp 189–205

Robling A, Stout S (2008) Histomorphometry of human cortical bone: applications to age estimation. In: Katzenberg M, Saunders S (eds) Biological anthropology of the human skeleton. Wiley, New York, pp 149–182

Rose D, Agnew A, Gocha T, Stout S, Field J (2012) Technical note: the use of geographical information systems software for the spatial analysis of bone microstructure. Am J Phys Anthropol 148:648–654

Ruth E (1953) Bone studies. II. An experimental study of the haversian-type vascular channels. Am J Anat 93:429–455

Schaffler M, Burr D, Jungers W, Ruff C (1985) Structural and mechanical indicators of limb specialization in primates. Folia Primatol 45:61–75

Sims N, Martin T (2014) Coupling the activities of bone formation and resorption: a multitude of signals within the basic multicellular unit. BoneKEy Rep 3:481

Singh I, Tonna E, Grandel C (1974) A comparative histological study of mammalian bone. J Morphol 144:421–438

Skedros J. (2002) Use of predominant collagen fiber orientation for interpreting cortical bone loading history: Bending vs. torsion. J Bone Miner Res 17:S307

Skedros J, Mason M, Bloebaum R (1994) Differences in osteonal micromorphology between tensile and compressive cortices of a bending skeletal system: indications of potential strain-specific differences in bone microstructure. Anat Rec 239:405–413

Skedros J, Su S, Bloebaum R (1997) Biomechanical implications of mineral content and microstructural variations in cortical bone of horse, elk, and sheep calcanei. Anat Rec 249:297–316

Skedros J, Sorenson S, Jenson N (2007) Are distributions of secondary osteon variants useful for interpreting load history in mammalian bones? Cells Tissues Organs 185:285–307

Skedros J, Kiser C, Keenan K, Thomas S (2011) Analysis of osteon morphotype scoring schemes for interpreting load history: evaluation in the chimpanzee femur. J Anat 218:480–499

Skedros J, Dayton M, Sybrowsky C, Bloebaum R, Bachus K (2006) The influence of collagen fiber orientation and other histocompositional characteristics on the mechanical properties of equine cortical bone. J Exp Biol 209:3025–3042

Skerry T (2006) One mechanostat or many? Modifications of the site-specific response of bone to mechanical loading by nature and nurture. J Musculoskelet Neuronal Interact 6:122

Tersigni-Tarrant M, Byrd J, Manabe J (2011) Test of osteon circularity as a method of human/non-human identification. American Academy of Forensic Sciences Meetings, Abstract H090, Chicago, Illinois, USA, pp 381

Urbanova P, Novotny V (2005) Distinguishing between human and non-human bones: histometric method for forensic anthropology. Anthropologie (1962) 43:77–86.

van Oers R, Ruimerman R, van Rietbergen B, Hilbers P, Huiskes R (2008) Relating osteon diameter to strain. Bone 43:476–482

Wolff J (1892) Das Gesetz der Transformation der Knochen.Berlin: A Hirschwald (Springer-Verlag published an excellent English translation of this monograph in 1986)